Arab J Sci Eng (2014) 39:5171–5184
DOI 10.1007/s13369-014-1179-3

RESEARCH ARTICLE - MECHANICAL ENGINEERING

Hardness and Wear Behaviour of Semi-Solid Cast A390 Alloy Reinforced with Al_2O_3 and TiO_2 Nanoparticles

I. El Mahallawi · Y. Shash · R. M. Rashad · M. H. Abdelaziz · J. Mayer · A. Schwedt

Received: 5 March 2013 / Accepted: 30 June 2013 / Published online: 3 June 2014

Abstract In this work, a series of castings of hypereutectic aluminium–silicon samples (A390) were prepared by rheocasting in a specially designed and built furnace unit allowing for the addition of the Al_2O_3/TiO_2 nanoparticles to the Al–Si slurry, with mechanical stirring. The microstructure features and the hardness of the cast samples were investigated, as well as the resistance to wear in laboratory tests. The results obtained in this work show enhancement in the micro-hardness and hardness of the Al_2O_3/TiO_2 nanodispersed hypereutectic A390 alloys, combined with improved wear resistance. The obtained results revealed that the introduction of Al_2O_3/TiO_2 nanodispersions together with the stirring effect induces a refining role, as significant refining was observed in the microstructure of the alloy. The results have also shown that modified intermetallic precipitates have appeared after adding the Al_2O_3/TiO_2 nanoparticles. Evidence for the formation of a combined (TiAlMgSi) oxide has been also presented in this work and its contribution in enhancement of wear resistance cannot be ruled out.

I. El Mahallawi (✉)
Department of Mining, Petroleum and Metallurgical Engineering, Faculty of Engineering, Cairo University, Cairo, Egypt
e-mail: ielmahallawi@bue.edu.eg; saiman@eng.cu.edu.eg

Y. Shash · R. M. Rashad
Department of Mechanical Engineering, Faculty of Engineering, Cairo University, Cairo, Egypt

M. H. Abdelaziz
Department of Mechanical Engineering, Faculty of Engineering, British University, El Sherouk, Egypt

J. Mayer · A. Schwedt
Gemeinshaftslabour, Aachen University, Aachen, Germany

Keywords Nanodispersion · Semi-solid processing · Hypereutectic Al–Si cast alloys · Hardness and wear

الخلاصة

تم في هذا البحث صب مجموعة عينات اسطوانية الشكل من سبيكة الألومنيوم – سليكون فوق اليوتكتيك (17% سليكون) من الحالة شبه الصلبة – السائلة (درجة حرارة 620 مئوية) بعد معالجتها بإضافة حبيبات حجم نانوي من أكسيد الألومنيوم وأكسيد التيتانيوم مع التقليب. ومن ثم تمت دراسة تأثير تلك المعالجة في البناء المجهري للسبيكة والصلادة ومقاومة البري باختبار معملي. وقد أظهرت النتائج زيادة الصلادة للسبيكة بعد المعالجة بحبيبات أكسيد الألمنيوم والتيتانيوم يصاحبها تحسن في مقاومة البري الميكانيكي مقاسا بدلالة الفقد في الوزن وشكل السطح المعرض للبري. وأظهرت الدراسة كذلك وجود تأثير ملحوظ في حجم مكونات البناء المجهري للسبيكة ممثلا في اليوتكتيك – وحبيبات السليكون الأولية. وأخيرا أظهرت النتائج تكوين مركب من أكسيد التيتانيوم – الومنيوم – مجنسيوم – سليكون في أثناء عملية التجمد للسبيكة.

1 Introduction

Hypereutectic Al–Si alloys are used in various automotive and aerospace industries due to some outstanding properties that they possess. The most important properties relevant to this work are high castability, abrasion resistance and excellent strength to weight ratio. Despite those characteristics, the mechanical properties of the hypereutectic Al–Si alloys are remarkably inferior because of the presence of primary silicon particles which crystallise in coarse and irregular shapes. These alloys solidify over a wide range of temperature during which the primary silicon forms and grows to large particles. The size of the primary silicon particles is controlled by the frequency of nucleation, whilst the morphology of eutectic silicon is dependent upon growth conditions. Haizhi Ye [1] has presented an overview of Al–Si-based alloys for engine applications where he has shown that fatigue failure and wear caused by surface delamination are the most impor-

tant causes for failure or end of life of engine parts. The main causes according to the analysis presented by Haizhi Ye [1] are the size and shapes (morphology) of the primary Si particles (PSPs).

The mechanical properties of hypereutectic Al–Si alloys are highly affected by the morphology, size, and distribution of both PSPs and eutectic silicon. The morphology of silicon particles are dependent on the solidification rate; as under normal casting conditions PSPs are very coarse and show star-like and other irregular shapes. Therefore, to improve the mechanical properties of the hypereutectic Al–Si alloys, size, distribution, and the morphology of PSPs and eutectic silicon should be controlled, as well as refining of the aluminium dendrites. The most important known technique for modification of the microstructure of the hypereutectic Al–Si alloy (A390) is to add phosphorous (P) as a refining agent. Gruzleski et al. [2] discussed this technique commonly used in the foundry, and showed that refinement of the primary silicon is achieved by the addition of phosphorous to the melt, though no effect was observed on the eutectic silicon. Gruzleski et al. [2] also highlighted that in phosphorous-modified hypereutectic Al–Si alloys, both coarse and unmodified eutectic silicon surrounding the refined primary silicon are still observed. A simultaneous effect of refining primary silicon and modifying eutectic silicon would be very beneficial for the properties of the hypereutectic Al–Si alloys. Though sodium (Na) and strontium (Sr) are used to achieve refinement of the eutectic silicon, unfortunately a combined effect does not happen at the same time due to chemical incompatibility of phosphorous with the other modifying chemicals such as strontium and sodium; this has been explained by Gruzleski et al. [2] to result from the formation of strontium phosphide or sodium phosphide upon the addition of strontium or sodium to phosphorous pre-refined alloys. Weixi et al. [3] have shown that the control of primary Si size to be in the range 10–20 μm by modifying the alloy with Nd which has resulted in a significant improvement in tensile strength and elongation % of the Al-15% Si hypereutectic alloy. CHEN Chong et al. [4] have studied the complex modification of P and rare earth metals RE and they have proven that an obvious modification and refinement of the primary silicon particles occurred.

Evidence of significant enhancement in strength and other properties of Al–Si cast alloys by incorporating nanoparticles have been recently presented, for example El-Mahallawi et al. [5,6] have shown that introducing Al_2O_3 nanoceramic particles to (A356) alloy cast in the semi-solid state with mechanical stirring has a beneficial effect on optimising strength–ductility relationship in these alloys, whilst Mazahery et al. [7] used stir casting with a modified treatment for the added particles and have also shown significant improvement in hardness, 0.2 % yield strength, UTS and ductility of (A356) alloy. Also, other studies have shown enhancement in the microstructure and mechanical properties of the hypereutectic Al–Si alloy (A390) by casting in the semi-solid state [8]. ZHAO and WU [8] prepared cast A390 in the semi-solid state and studied its cast and T6 heat-treated condition where they found that the semi-solid casting results in fine and uniform microstructure where the average size of primary Si spheroids was found to be 20–30 μm, combined with improved tensile strength, ductility, hardness and wear resistance. TEBIB et al. [9] have developed a novel rheoforming process to investigate semi-solid processing of hypereutectic A390 alloys using a combination of the swirl enthalpy equilibration device and isothermal holding, they managed to improve the process-ability of semi-solid slurries for A390 alloy and they reported evidence of enhancement of the microstructure. They have also shown that primary silicon in the semi-solid microstructure can be refined by phosphorous additions, but refinement of primary silicon and modification of eutectic silicon cannot be achieved simultaneously by phosphorous and strontium additions. Dehong et al. [10] have also presented electromagnetic stirring of semi-solid Al–Si hypereutectic alloys as an appropriate method for refining the PSPs.

Rohatgi et al. [11] have predicted the significant role of producing Al–Si ceramic composites for bearings, pistons, cylinder liners, etc. leading to savings in materials and energy. Recently, Rosso [12] presented a review on routes and properties of ceramic reinforced metal composites where it was shown that adding reinforcing particles to the liquid phase in casting processes usually results in poor properties obviously due to the defects arising from high melting temperatures at which the reinforcement is usually added. The advantages associated with using rheo-casting were also described from which it could be concluded that this method exhibits several advantages over the first method such as lower porosity content, good distribution of reinforcements, and less harmful interfacial reactions. Moreover, the enhanced viscosity of the semi-solid processing would serve to improve the ceramic particle/melt wettability and entrap or capture the reinforcement material physically. It has also been proven [13–15] that casting in semi-solid conditions results in modification of the dendritic columnar structure into a smaller and equiaxed globular grain arrangement.

Kim et al. [16] described in detail the combined role of nanoparticles dispersion and semi-solid processing in producing equiaxed particles in favour of dendritic structures. This has been attributed to their combined effect on causing the growth and heat flux directions to be the same, and hence promoting the nucleation of the equiaxed grains in a random matter. In this case, the last traces of the remained liquid (including the nanoparticles) are blocked among the branches and preferentially solidified, capturing the nanoparticles within the grain itself, rather than only on the grain boundary.

However, till the time of completing this research no reported work has been found on the effect of using nano-

sized ceramic particles on the microstructure and mechanical properties or wear performance of the hypereutectic Al–Si alloy (A390).

It is difficult to obtain uniform dispersion of the ceramic particles in liquid metals due to poor wettability in the metal matrix, and the large surface-to-volume ratio of the added particles. These problems induce agglomeration and clustering, as presented by Rosso [12]. In two-phase (solid–liquid) processes, which are called rheo-casting or compo-casting, the reinforcements are added to the metal, whilst it is in the semi-solid state. Micro-sized alumina (Al_2O_3) and other oxide particles like TiO_2 etc. have been used as reinforcing particles in Al-matrix. Alumina has received attention as a reinforcing phase as it is found to increase the hardness, tensile strength and wear resistance of aluminium metal matrix composites. Rohatgi et al. [11] have found based on an extensive study that dispersed particles such as alumina result in particle refinement of both eutectic and primary Si.

The main idea presented here is to combine effects from semi-solid casting with those from nanodispersion to produce a modified Al–Si hypereutectic cast alloy. In this work, rheo-casting process was used combined with the addition of nanoceramic particles of aluminium and/or titanium oxides. Aluminium oxide (γ-Al_2O_3) was chosen in this work due to its compliance with the requirements of reinforcing material, as presented by Huda et al. [17], as follows: not forming intermetallic compounds with the matrix elements, and being physically and chemically compatible as possible with the matrix. γ-Al_2O_3 is FCC, it has a higher density than the aluminium matrix (3.6 g/cm^3) which reduces its chances to float, and it has a higher Young Modulus as compared to the original aluminium matrix (388 GPa).

2 Materials and Experimental Procedures

2.1 Materials

The base metal for the produced material was selected to be the hypereutectic Al–Si alloy A390, the analysis of which is given in Table 1. This alloy was chosen for its wide use in automotive and aeronautical applications.

The materials used for reinforcement were Al_2O_3 and TiO_2 ceramic nanoparticles (prepared at the Central Metallurgical Research and Development Institute, CMRDI) with average particle size of 50 nm, the description of which is given in Table 2.

Table 1 Chemical composition (in wt.%) of the base alloy

Alloy	Chemical composition (wt.%)							
	Si	Mg	Fe	Cu	Ti	Zn	Mn	Al
A390	17	0.45	0.5	4.5	0.2	0.1	0.1	Bal.

Table 2 Properties of Al_2O_3 and TiO_2 reinforcement particles

Reinforcement	γ-Al_2O_3	TiO_2
Density (g/cm^3)	3.60	4.23
Crystal structure	FCC	Tetragonal
Appearance	White solid	White solid
Young's modulus (GPa)	380	244
Average size (nm)	50	50
Melting point (°C)	2,054	1,870
Thermal conductivity (W/m K)	25.08[a]	11.7
Coefficient of thermal expansion (10^{-6} m/m K)	5.4	9

[a] CRC Materials Science and Engineering Handbook, p.281

2.2 Processing

2.2.1 Furnace and Mould

The samples prepared for this work were prepared in an electrical resistance furnace that was designed and constructed for this research work for preparing the nanodispersed alloys. It consists of a lift out graphite crucible of max. 8 kg capacity and is operated by a heating system equipped with a control unit with a thermocouple for controlling the temperature up to 1,200 °C [6]. An external stirring mechanism of variable height and driven by a motor of 3,000 rpm was attached to the system and allowed to melt through an opening in the top of the furnace. The stirrer was made of a stainless steel rod with four pitched blades weld to its lower end. The design of the impeller was to promote axial flow. A metallic mould made of cast iron with ten cylindrical mould cavities of diameter 20 and 150 mm height was used for casting the test specimens [6].

2.2.2 Melting, Adding Powders and Pouring

A charge of 3 kg of the base alloy was introduced to the crucible and heated up to the melting temperature (655 °C). After reaching the liquid state, the melt was degassed with either argon or hexachloroethane degasser tablet, to get rid of gases. After degassing, the melt was brought down to the semi-solid state (605–610 °C) and hence the addition of Al_2O_3 and TiO_2 nanoparticles, prepared in packages of aluminium foil and preheated to about 200 °C, took place. The packets were added to the melt through the opening in the top of the furnace one packet after the other, simultaneously with mechanical stirring for 1 min at 1,000 rpm. Table 3 summarises the fabrication conditions of the composites prepared in this investigation. Cast samples were poured in the

Table 3 List of produced alloys and fabrication conditions

Alloy	Additions/designations	Melting conditions	Pouring conditions
Monolithic	0 %/A390	Degassing in liquid state, adding nanoparticles and mechanical stirring for 1 min in semi-solid state	Pouring in semi-solid state at 600 °C
A1-600	1% Al_2O_3/(A1-600)		
AT-600	0.5 % Al_2O_3 + 0.5 % TiO_2/(AT-600)		
AT1.5-600	1 % Al_2O_3 + 0.5 % TiO_2/(AT1.5-600)		
AT-645	0.5 % Al_2O_3 + 0.5 % TiO_2/(AT-645)	Degassing in liquid state, adding nanoparticles and mechanical stirring for 1 min in liquid state	Pouring in liquid state at 645 °C

prepared mould without additions and with additions of different investigated percentage additions. The prepared cast samples were hence used for further investigation.

2.3 Microstructure characterization

2.3.1 Optical Microscopy

Representative sections from the cast samples were cut into three pieces: the first from the top, the second from the middle and the third from the bottom. Samples were wet ground on a rotating disc using silicon carbide abrasive discs of increasing fineness (120, 180, 220, 320, 400, 600, 800, 1,000, and 1,200 till 4,000 grit). Then, they were polished using 1 and 3 μm diamond paste. This was followed by polishing and micro-polishing using a vibrator polishing machine. The microstructure examination was carried out using optical metallurgical microscope equipped with a high resolution digital camera for investigating the microstructure. The microstructure features, namely the size of the silicon particles in the largest dimension, the dendritic arm length, and the interlamellar spacing in the eutectic silicon phase, were evaluated by conducting more than 30 readings on all the investigated samples. The measurements were made using "JMicroVision v1.27" image analyser.

2.3.2 Scanning Electron Microscopy (SEM)

The morphology of the primary phases and the eutectic structure was further investigated using a JSM-7000F FEG-SEM using back scattered electrons (BSE) technique. Samples were prepared by grinding followed by polishing and micro-polishing using a vibration-polishing machine. Some selected samples for SEM examination were prepared by ion polishing using argon ions using a Jeol SM09010 cross-section polisher.

2.4 Mechanical and Wear Characterisation

The hardness and the micro-hardness of the investigated materials were measured as follows:

2.4.1 Micro-Hardness Test

The micro-hardness examination was carried out using Polyvar optical metallurgical microscope equipped with a high resolution digital camera and Vickers micro-hardness tester using the load of 0.98 N. The reported results are the average of a minimum of five readings.

2.4.2 Hardness Test

The overall hardness was also measured by a Brinell hardness testing machine using 2.5 mm diameter hardened steel ball and 1,839 N applied load. The reported results are the average of a minimum of seven readings.

2.4.3 Pin-On Disc Wear Test

Wear test was conducted using a pin-on-disc tribometer testing machine at 265 rpm (1 m/s) with two different applied loads: 3 and 4 N for 15 and 30 min, respectively. The cylindrical shaped samples were 10 mm round and 20 mm high and were run on a 70-mm steel disc of 63 Rc hardness. The conditions were selected to be harsh for aluminium alloys and the wear test was conducted in two different conditions as follows:

1. Running speed of 1 m/s (265 rpm), load 3 N, and for 30 min long.
2. Running speed of 1 m/s (265 rpm), load 4 N, and for 15 min long.

3 Results and Discussion

3.1 Microstructure

3.1.1 Optical Microscopy

The microstructure of the investigated hypereutectic Al–Si alloys consists of three different phases; namely: primary silicon particles, α-Al in dendritic or equiaxed form (as a result of semi-solid processing), as well as binary Al–Si eutectic

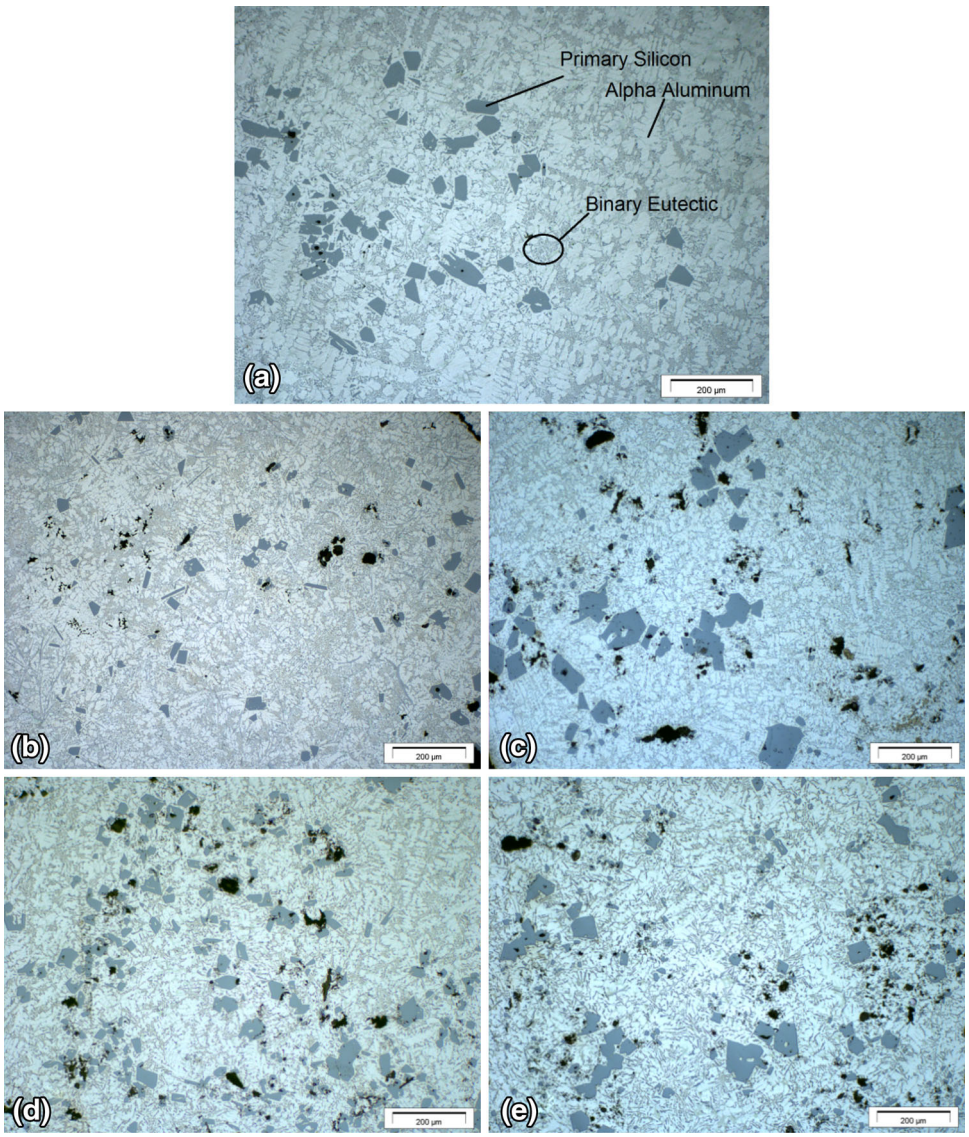

Fig. 1 Microstructures of **a** monolithic cast A390 alloy, **b** A390 containing 1 %Al_2O_3 cast in semi-solid, **c** 0.5 % Al_2O_3-0.5% TiO_2 cast in semi-solid, **d** 0.5% Al_2O_3-0.5 TiO_2 cast in liquid, **e** 1 % Al_2O_3-0.5% TiO_2 cast in semi-solid

structure, as shown in Fig. 1. The morphology of the primary silicon in all the studied samples is shown to remain polygonal, except for the sample containing 1 % Al_2O_3 where little primary needle like silicon particles were spotted. Moreover, it is shown from Fig. 2 that the eutectic silicon has two morphologies, the first one shows a fine skeleton network with Chinese script morphology, mainly present in spaces between α-Al dendrite arms, whilst the second one is flake like and can be found around the primary silicon particles.

Figures 3 and 4, and Table 4 show the influence of the Al_2O_3/TiO_2 nanoparticles on some microstructure features, namely; dendritic arm length, interdendritic arm spacing and interlamellar spacing in the eutectic silicon structure, as well as the size of the primary Si particles.

The narrowing of the range of scatter in the size of the micro-constituents (Fig. 4; Table 4) associated with the processing method developed in this work is obvious. Also,

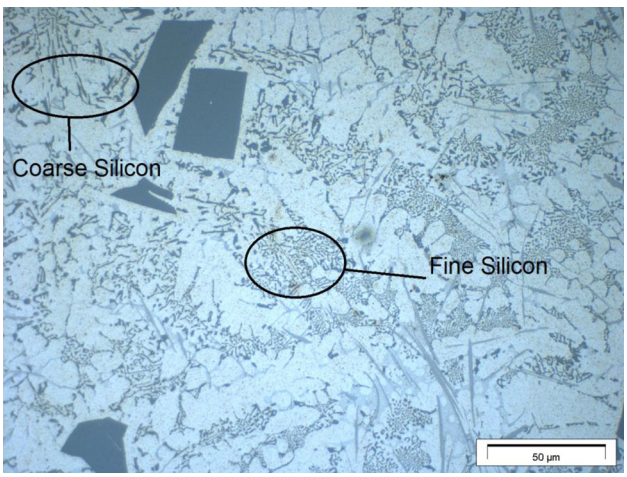

Fig. 2 Eutectic Silicon morphologies—fine, skeleton network with Chinese script morphology—flakes surrounding primary silicon particles

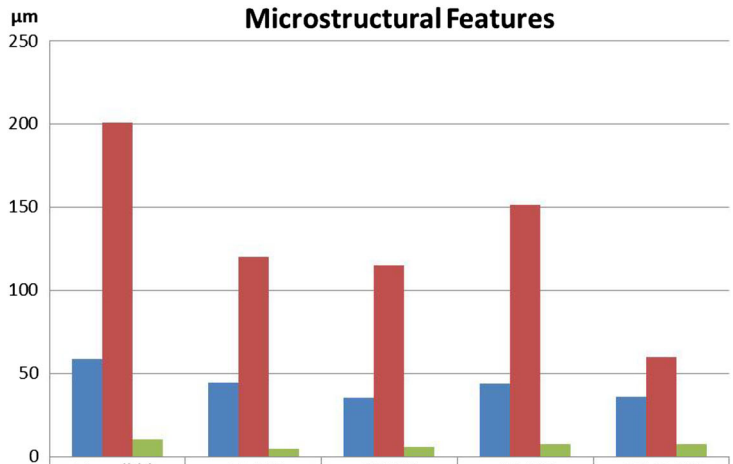

	Monolithic	A1-600	AT-600	AT-645	AT1.5-600
Interdendritic arm spacing (µm)	58.83	44.50	35.60	43.82	36.00
Dendrite arm length (µm)	200.72	119.94	114.94	151.38	60.00
Interlamellar spacing (µm)	10.64	4.74	5.78	7.42	7.54

Fig. 3 Values of interdendritic arm spacing, dendrite arm length, and interlamellar spacing for the investigated samples

an overall trend for size decrease was apparent in the studied samples except for the material (AT-600) containing 0.5 % Al_2O_3-0.5 % TiO_2 cast in semi-solid state which revealed a wide scatter in the silicon particles size, though these results maybe an effect of non-homogeneous processing conditions. The sample material (AT-645) containing 0.5 % Al_2O_3-0.5 % TiO_2 cast in liquid state has shown relatively higher content of refined primary silicon particles.

The morphology of the eutectic silicon is dependent on growth conditions, whilst the morphology of the primary silicon is controlled by increasing the number of nuclei through increasing the frequency of nucleation. This explains the reason behind the significant refining effect observed upon adding the Al_2O_3 nanoparticles since they act as nucleating agents increasing the number of primary formed Si particles upon the solidification of the alloy. The significant role of TiO_2 in refining the aluminium phase is evident from Table 4.

3.1.2 Scanning Electron Microscopy

Figures 5 and 6 show typical BSE images obtained for the alloys containing 1 % Al_2O_3 and 1%Al_2O_3 + 0.5 % TiO_2, respectively, cast in semi-solid state after ion polishing. The EDX analysis of the various micro-constituents and precipitates was identified by BSE as shown in the figures confirming the presence of primary silicon phase, α-Al dendrites, and the eutectic structure mainly consisting of binary Al–Si eutectic. The figures also demonstrate the presence of the traditional intermetallic compounds that form in hypereutectic Al–Si alloys namely; $CuAl_2$, $Cu_2Mg_8Si_6Al_5$, and Al_5FeSi. Also, Al_2O_3 and TiO_2 particles were observed in some regions (Fig. 7). Khalifa et al. [18] have referred to the role of the Al_2O_3 precipitates in acting as nucleating agents in Al alloys. Figure 7 also shows the presence of Al_2O_3 in the sample containing 1 %Al_2O_3-0.5 %TiO_2 cast in semi-solid state after ion polishing. Though the analysis of the TiO_2 particles shown in Fig. 7 indicates the presence of other constituents: Al, Mg, Si, Cu, they may be either coming from the matrix due to the small size of the analysed point, or resulting from dissolution of some of these elements to form a combined TiAlMgSi oxide. The presence of Ti in the analysis may also suggest the formation of TiAlSi intermetallic phase on small scales, as reported before by Tong Gao et al. [19], though no evidence of this precipitate has been confirmed through this work. However, it should still be stated that Al_2O_3 nanoparticles appeared mostly agglomerated around the pores and at the end of dendrite arms. The results obtained by examining the cross-section polished samples confirmed that the particles would be pushed by the solidification front during the dendrite solidification, as reported earlier [5,6].

3.2 Hardness

Table 5 presents the micro-hardness values for the identified phases in the newly developed alloys with different nanoadditions. A significant variance is evident between the hardness values of the primary silicon particles and the other phases, i.e. eutectic structure, and α-Al. In several occasions, the Si particles were crashed under the indentation load during the hardness test which made the measurement process uneasy. Though the micro-hardness of the primary silicon phase is shown to be significantly high in all samples, great variations were found according to the shape of the particles, therefore, the reported values were chosen to be those for polygonal-shaped particles with sizes in the range of 30 µm only. The highest values were associated with the presence of 0.5 %

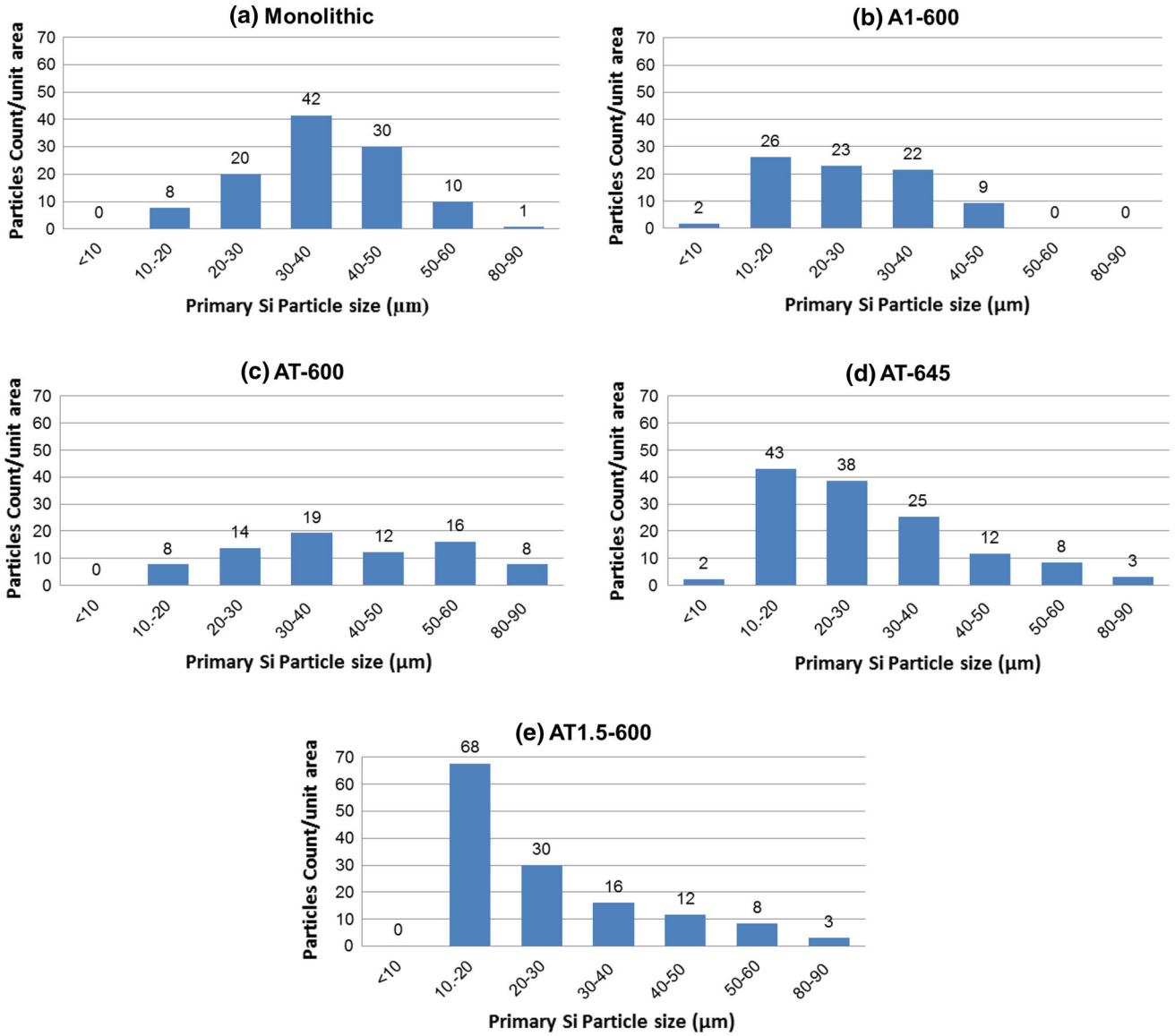

Fig. 4 Primary silicon size analysis for a fixed unit area: **a** monolithic cast A390 alloy, **b** A390 containing 1 %Al_2O_3 cast in semi-solid, **c** 0.5 % Al_2O_3-0.5 % TiO_2 cast in semi-solid, **d** 0.5 % Al_2O_3-0.5 % TiO_2 cast in liquid, **e** 1 % Al_2O_3-0.5 % TiO_2 cast in semi-solid

Table 4 Influence of nanoparticles additions on the dendritic arm length, interdendritic arm spacing, interlamellar spacing and primary Si for the studied samples

Alloy A390	Interdendritic arm spacing (µm)		Dendrite arm length (µm)		Interlamellar spacing (µm)		Primary Si particles
	Average (µm)	Data range (µm)	Average (µm)	Data range (µm)	Average (µm)	Data range (µm)	% Si particles in size range (µm)
Monolithic	58.83	41.6–80	200.72	173.6–232	10.64	6.8–13.8	(83 %) 20–50
A1-600	44.50	31.5–53	119.94	106.7–138	4.74	3.2–7.36	(86.5 %) 10–40
AT-600	35.60	28–40	114.94	91.7–143	5.78	4.3–7.3	(79 %) 20–60
AT-645	43.82	40.22–52	151.38	128.9–175	7.42	5.025–10.62	(81 %) 10–40
AT1.5-600	36.00	32–40	60.00	56–64	7.54	4.22–10.8	(83 %) 10–40

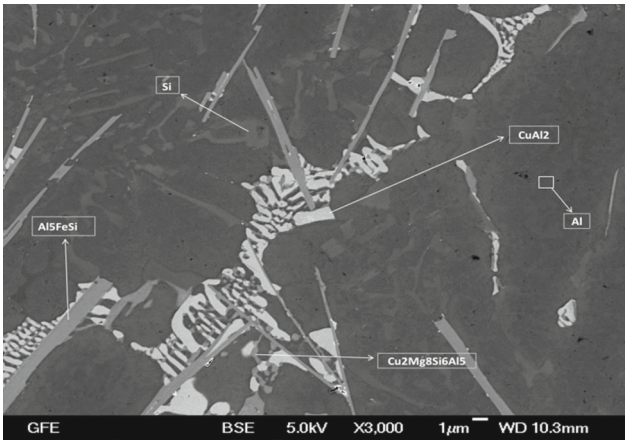

Fig. 5 BSE image of 1 % Al_2O_3 cast in semi-solid state showing the main microstructure constituents appearing in the as-cast state

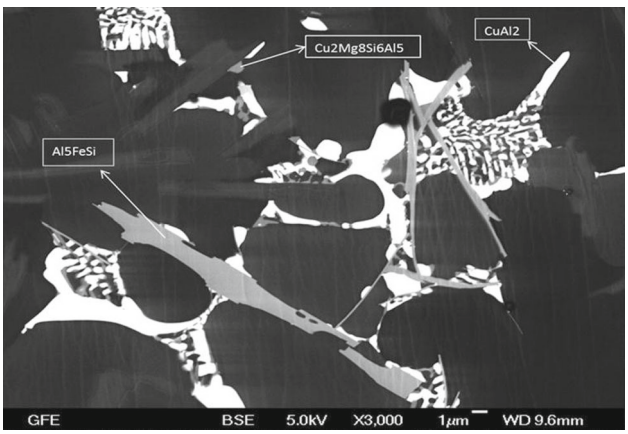

Fig. 6 BSE image of 1 % Al_2O_3-0.5 % TiO_2 cast in semi-solid state showing different intermetallic compounds appearing in the as-cast state

TiO_2 combined with the Al_2O_3, as the two alloys containing 0.5 % TiO_2 showed the highest micro-hardness of the primary Si phase, whereas, the addition of Al_2O_3 nanoparticles alone did not show a significant effect on the micro-hardness of the silicon particles.

By combining the micro-hardness results presented in Table 5 with the refining results presented in Table 4 and Figs. 3 and 4, it can be shown that the addition of Al_2O_3 nanoparticles alone produces refining of the silicon particles and insignificant change of micro-hardness, whereas, the combined addition of Al_2O_3 and TiO_2 nanoparticles results in a refining effect of the primary Si particles, as well as a significant increase of their micro-hardness. This may be explained by the thermal properties of both dispersions: the higher thermal conductivity of the Al_2O_3 particles as compared to the TiO_2 particles would promote local subcooling conditions promoting the refinement process; whilst the higher thermal expansion of the TiO_2 nanoparticles as com-

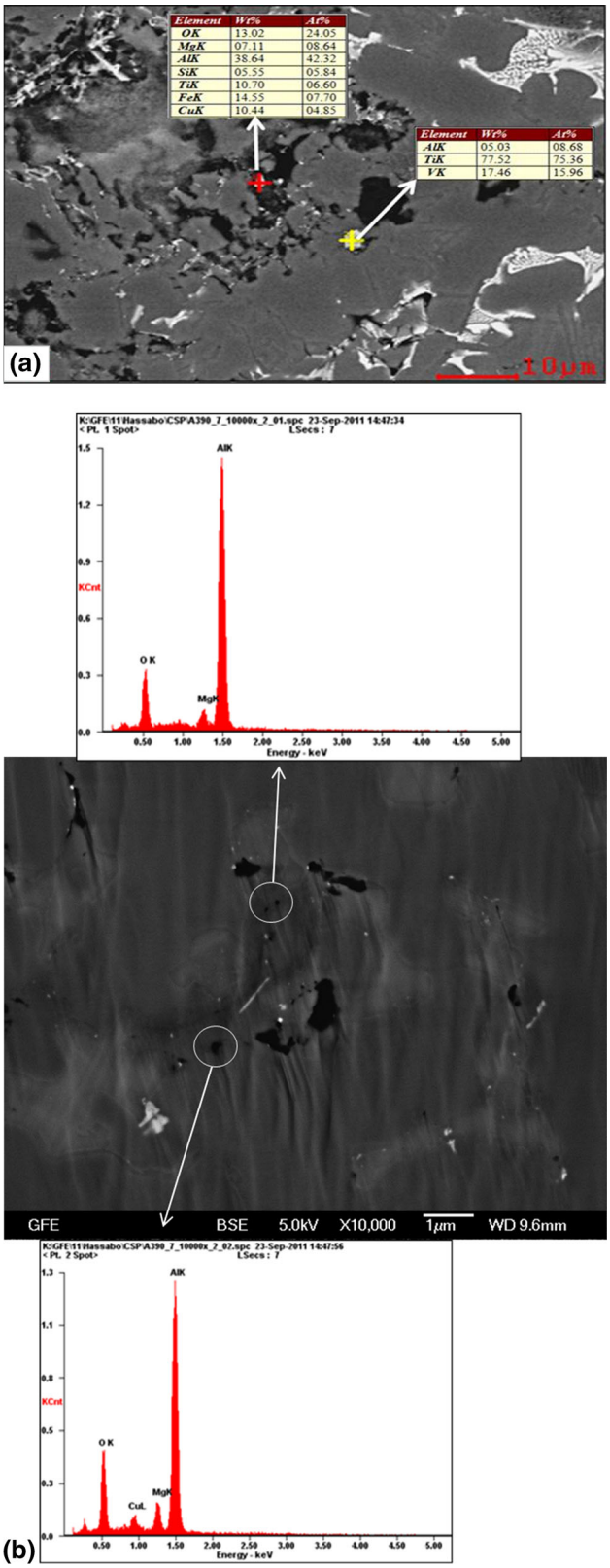

Fig. 7 **a** Sites of nanodispersions of the sample containing 1 % Al_2O_3 and 0.5 % TiO_2 cast in semi-solid state, **b** BSE image for the ion polished alloy containing 1 % Al_2O_3 and 0.5 % TiO_2 cast in semi-solid state

Table 5 Micro-hardness values

	Monolithic	A1-600	AT-600	AT-645	AT1.5-600
Primary Si (HV)	1,762	1,773	2,149	2,165	2,033
Eutectic structure (HV)	169	185	184	173	170
α-Al (HV)	159	169	176	165	139

pared to the Al_2O_3 nanoparticles would create local strained zones that would cause the rise of the hardness. The results also show that the change in the size of the Si particles does not affect the hardness values significantly.

Figure 8 shows a comparison of the overall hardness of the investigated material with different additions. It can be seen from Fig. 8 that an overall increase in the hardness values occurs upon the addition of the nanoparticles. It can be also seen from Fig. 8 that the highest overall hardness is observed for the alloy AT-600 (containing 0.5 % Al_2O_3 + 0.5 % TiO_2). The results are compatible with the results obtained from the micro-hardness test where the hardness of the primary Si particles was the highest for this alloy. It is also clear that the Si particles seem to be significantly affecting the overall hardness of this alloy. It is also seen from Table 5 that the alloy AT-600 (containing 0.5 % Al_2O_3 + 0.5 % TiO_2) has the highest micro-hardness for the Al phase.

3.3 Wear Behaviour

3.3.1 Results of Wear Test

Figure 9 illustrates the wear test results as compared to the hardness values of the developed material, from which it is shown that the sample A1-600 containing 1 % Al_2O_3 cast in semi-solid state has exhibited the least wear for the conditions of 4 N, 1 m/s, and 15 min, whereas, the alloy AT-600 containing 0.5 % Al_2O_3-0.5 % TiO_2 and cast in semi-solid state has shown the least wear in the condition of 3 N, 1 m/s, and 30 min. The samples without wear results have completely disintegrated during the test. Though the alloys that exhibited the least wear are not those undergoing the greatest refining effect, the improvement in wear resistance is shown to be in good agreement with the hardness results.

The results obtained in this work have shown enhancement in the wear rate in g/s of the newly developed materials after the dispersion of the nanoparticles in the semi-solid state, with the least reported wear losses for the alloys A1-600 and AT-600. Those results seem to be in line with the reported increase in hardness for those two alloys containing nanodispersions. Figure 9 also shows that the size of the primary silicon particles for the two alloys showing highest wear resistance is significantly characterised by a pattern covering the full range of particles sizes, unlike other conditions showing clustering around one size range. The effect of structure modification has been previously reported, where an improvement in wear properties of Al–Si alloys was found after being refined and modified. Alireza and Frank [20] developed a Mg-treated Al–Si–Cu–Mg alloy by rheo-casting with variable Mg contents and they discussed the effect of Mg treatment on the microstructural characteristics of the 390 hypereutectic aluminium-silicon alloy. Hence, Alireza et al. [21] have studied the wear behaviour of the alloys and have shown improvement in the wear of A390 alloy after refining and modifying its structure by controlled Mg additions and T6 heat treatment. However, this is the first time where refining due to nanodispersion is reported. The deviation in alloy AT1.5-600 may be explained by the significant refining of the Si particles as shown in Fig. 4e.

The highest hardness in this work was found to be that of the material AT-600 which showed the majority of silicon

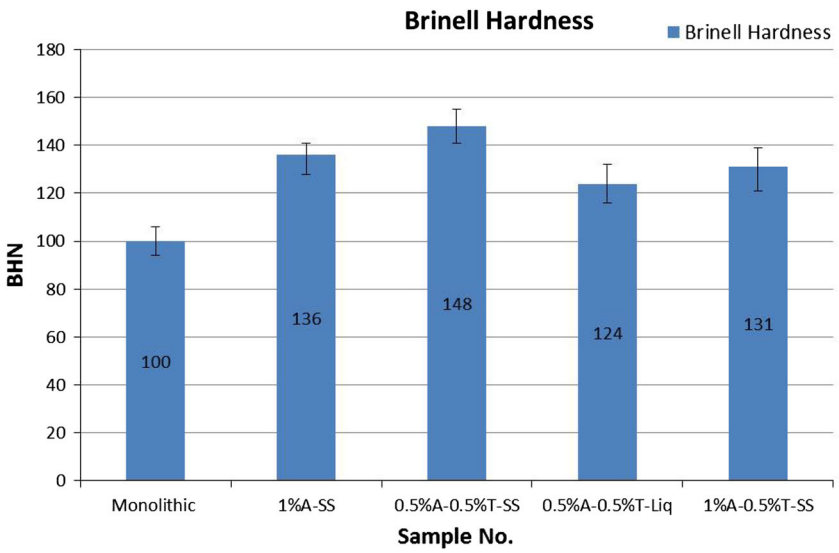

Fig. 8 Change in hardness with nanoparticles additions

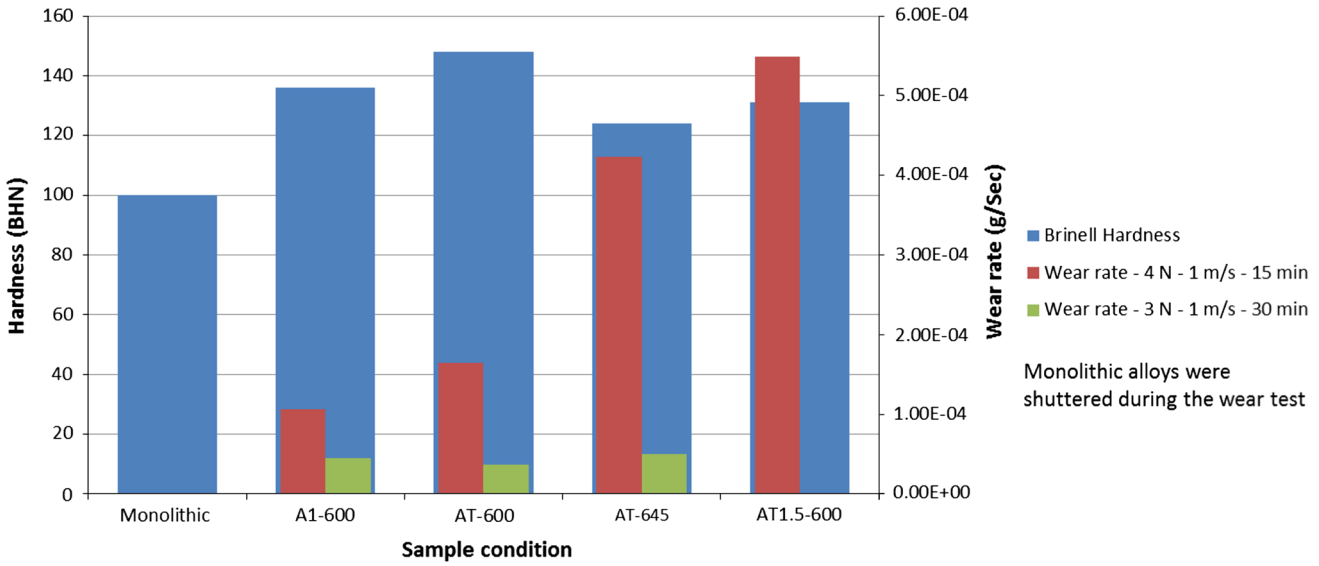

Fig. 9 Wear rate against Brinell hardness and sample manufacturing conditions

particles (79 %) to be in the range 20–60 μm, followed by the alloy A1-600 which showed the majority of silicon particles (86.5 %) to be in the range 10–40 μm. It is also worth noticing that those two conditions showed the least loss in wear rates for both testing conditions. This raises a debate on if the refinement of PSPs in hypereutectic alloys has a positive effect on its wear properties, and if it is the total amount of silicon or the morphology which determines the wear properties.

The high difference in wear rates for the two wear tests is also attributed to the load and sliding time, when the test lasted for longer time (30 min), at 3 N the materials showed a general better performance than the results for the test that lasted for 15 min at 4 N. This reduction in wear rates may possibly be a result of higher contamination of sliding surfaces with oxide layer. The presence of the oxide layer reduces the direct metallic contact between the two sliding surfaces and hence reduces the adhesive wear that may be initiated. Also exposing the material to wear test in dry conditions may lead to increase in temperature and this increase in temperature will participate in softening the aluminium matrix leading to higher plastic deformation, which may have been the case at the higher load.

3.3.2 SEM Study of the Worn Surfaces

The SEM study of the worn surfaces has revealed many interesting observations. Figure 10 shows the SEM image for the monolithic sample, which experienced a complete destruction during the wear test; from which it is noticeable that the dominant wear mechanism was a combination of adhesion and delamination mechanisms, evidence of plastic deformation is also observed on the worn surface. Since the wear test was conducted in dry conditions, increase in temperature may have led to metal softening causing the severe plastic deformation and delamination experienced.

Alireza et al. [21] have studied and identified the features of the worn surfaces of a hypereutectic Al–Si Mg-treated alloy and have attributed wear to the debonding of large primary Si particles at their interface with the matrix. They concluded that the debonding of primary Si particles from a softer matrix affects the wear rate greatly, than if the matrix was harder causing particle fragmentation rather than pulling away.

Figure 11 illustrates the worn surface for the alloy containing 0.5 % Al_2O_3-0.5 % TiO_2 cast in semi-solid state, from which it appears that a combination of delamination and scoring is the main wear mechanism, also the image shows some regions of mild wear where plastic deformation was observed. Figure 12 shows the worn surface for the alloy containing 1 % Al_2O_3 where almost the same wear mechanism can be witnessed, also some debris can be observed on the surface indicating probability of abrasive wear occurrence.

Figures 13 and 14 show other SEM pictures for the worn surfaces of the specimens which have undergone relevantly higher wear loading conditions at shorter time for the alloys containing 0.5 % Al_2O_3-0.5 % TiO_2, and 1 % Al_2O_3 cast in semi-solid state, respectively. Similar features to those in Figs. 11 and 12 seem to dominate the worn surface which shows mild wear regions side by side to delamination and scoring wear. By comparing the worn surfaces of the monolithic alloy with those of nanodispersed alloys apparent differences can be witnessed and these differences are good explanations for the differences in wear rate values; as deep grooves with excessive plastic deformation can be seen on

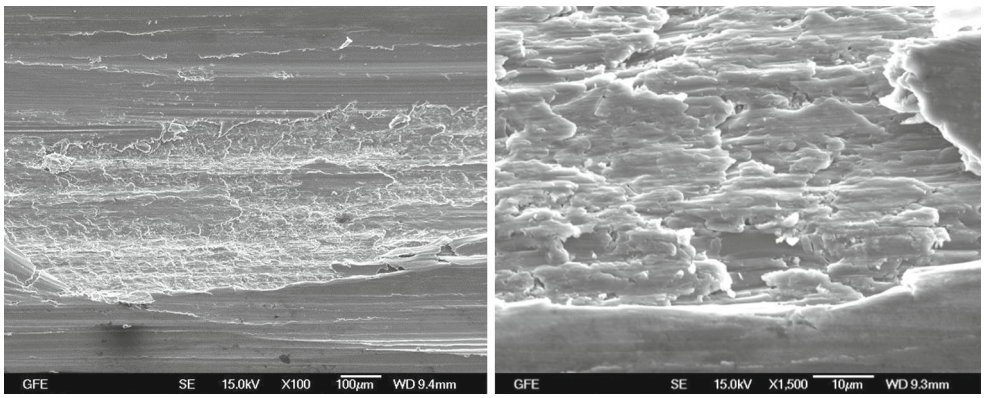

Fig. 10 SEM image of worn surface for the monolithic sample: 3 N, 1 m/s, and 30 min. showing sever delamination, plastic deformation and adhesive wear

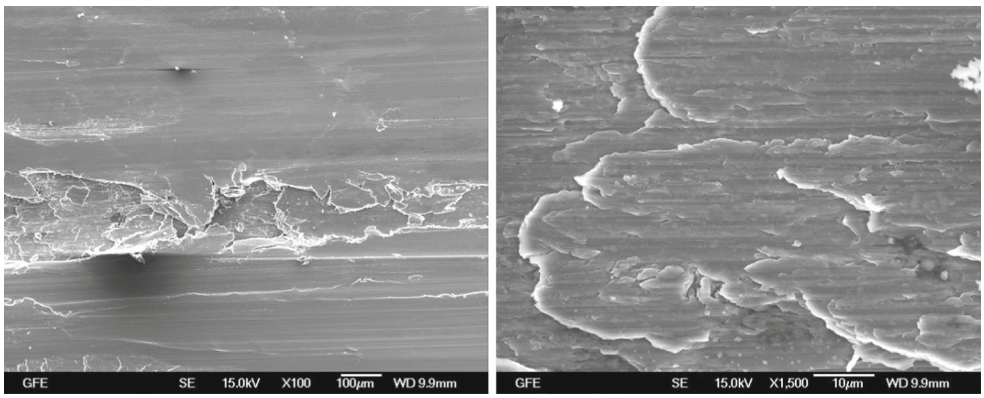

Fig. 11 SEM image of worn surface for the alloy containing 0.5 % Al_2O_3-0.5 % TiO_2 cast in semi-solid state at 3 N, 1 m/s, and 30 min showing less plastic deformation and adhesive wear

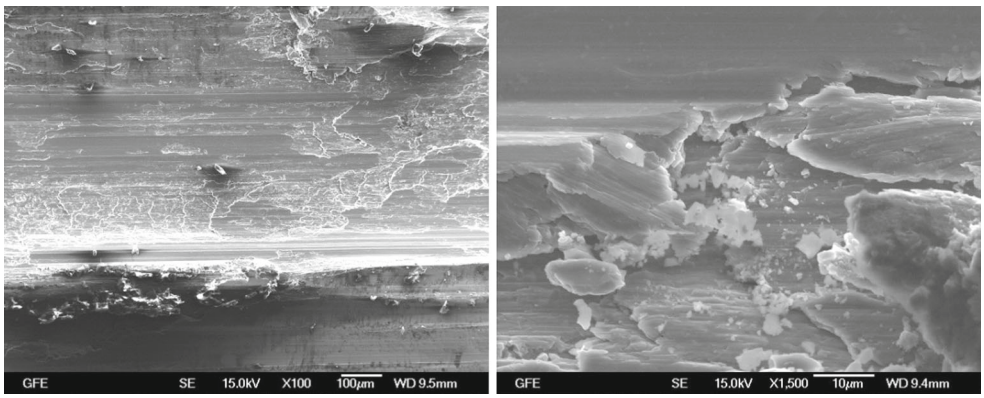

Fig. 12 SEM image of worn surface for the alloy containing 1 % Al_2O_3 cast in semi-solid state at 3 N, 1 m/s, and 30 min showing plastic deformation, and adhesive wear

the worn surface of the monolithic alloy whilst those grooves seem to be milder on the surfaces of the nanodispersed alloys. ChandrasheKhairaiah and Kori [22] have shown that after refining and modifying the structure of Al–Si eutectic alloys, the worn surfaces revealed the formation of less amount of adhesive wear.

The increase in the hardness of the Al_2O_3/TiO_2 nanodispersed hypereutectic A390 alloys, combined with improved wear resistance is evidenced in this work. Though the enhancement in wear resistance found in this work was the highest for the alloy A1-600 reinforced with 1 % Al_2O_3 nanoparticles with 86.5 % of the primary Si size in the range

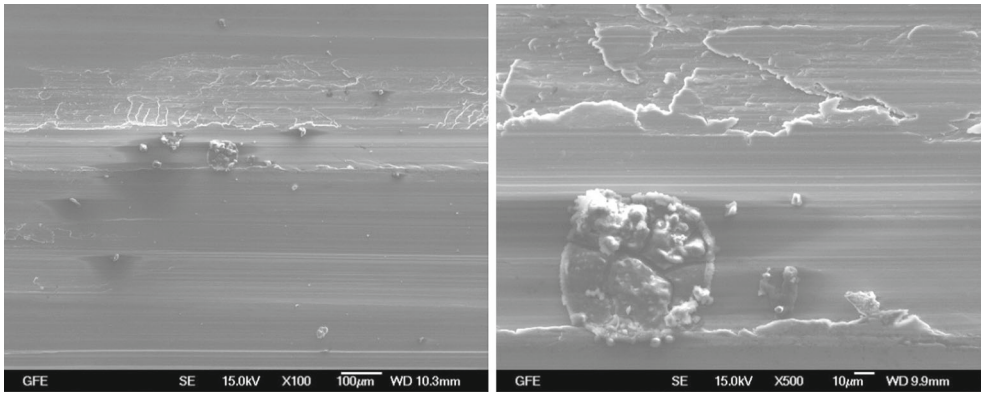

Fig. 13 SEM image for worn surface of the alloy containing 0.5 % Al_2O_3-0.5 % TiO_2 cast in semi-solid state at 4 N, 1 m/s, and 15 min showing less evidence of damage by adhesive wear

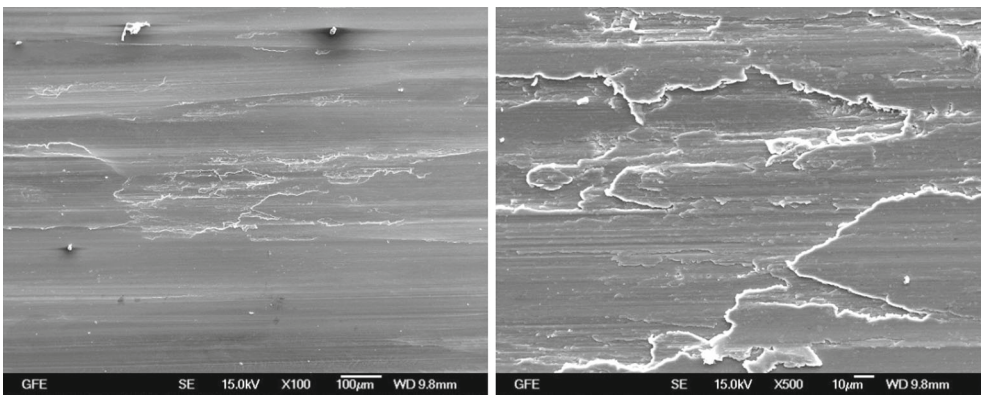

Fig. 14 SEM image for worn surface of the alloy containing 1 % Al_2O_3 cast in semi-solid state at 4 N, 1 m/s, and 15 min showing less evidence of damage by adhesive wear

10–40 μm and hardness of 138 HV at 4 N test load for 15 min, the results changed at 3 N test load for 30 min condition where the alloy AT-600 reinforced with 0.5 % Al_2O_3 and 0.5 % TiO_2 with 79 % of the primary Si size in the range 20–60 μm and hardness of 145 HV showed the least amount of wear. In both cases, the enhancement in wear resistance was related to the finer silicon particles (at the high test load 4 N), and the highest hardness (at the lower test load 3 N). The observed increase in the hardness of the A390 nanodispersed alloy and the micro-hardness of the primary silicon particles associated with the presence of Al_2O_3/TiO_2 nanoparticles suggests a misfit effect in the lattice parameter of the Si-rich phase, due to cooling-induced changes caused by the difference between the coefficients of thermal expansion between the Si-rich phase of the primary silicon particles (3×10^{-6} m/m K) and the Al_2O_3/TiO_2 nanoparticles (see Table 2), resulting an increase in the hardness of the first. Starink et al. [23] have developed a model describing the cooling-induced changes in Al–Si alloys, wherefrom the expected increase in hardness from added ceramic Al_2O_3 particles was made. Also, the enhancement in the micro-hardness of the Al phase in the Al_2O_3/TiO_2 nanodispersed alloy suggests enhanced dislocation generation and reduced subgrain size owing to the presence of the nanoparticles.

ChandrasheKhairaiah and Kori [22] have attributed the enhancement in the wear performance of Al–Si alloys to the conversion of coarse columnar α-Al dendrites to fine equiaxed dendrites, and changes of plate-like eutectic silicon to fine particles. Alireza et al. [21] have attributed improvement in the wear characteristics of A390 alloy to refining and modifying the morphology of PSPs structure by controlled Mg additions and T6 heat treatment. In this work, the enhancement in the wear resistance of the studied nanodispersed hypereutectic Al–Si alloy is attributed to refined structures of eutectic and primary Si, combined with morphological modification and equiaxed Al dendrites resulting from the semi-solid processing. A significant increase in hardness has occurred accordingly. Also, evidence for the formation of a combined TiAlMgSi oxide has been also presented in this work and its contribution in enhancement of wear resistance cannot be ruled out.

Various researchers have studied the wear behaviour of particulate reinforced aluminium matrix composites with the particulates ranging in size from microscale [24–26] to submicron scale [27]. In all cases, the wear mechanism was by delamination and abrasion at mild conditions, and adhesion and delamination at severe conditions. It has been reported [25] that there is a critical transition load above which severe wear caused by adhesion takes place, both the abrasive and adhesive wear rates were found to increase with increasing particle volume fraction and particle size. It was also shown [25] that the composites reinforced with $A1_2O_3$ particles show better wear resistance owing to the better bond strength in Al_2O_3-reinforced composites, however, the increase in adhesive wear rate associated with higher volume fractions and larger particles sizes was attributed to a higher possibility of crack initiation. It was suggested [26] that the volumetric wear decreases with the particle size of the reinforcement particulates. The results provided by this work show that using nanoparticles of Al_2O_3 would reduce the possibility of crack initiation and yet raise the shear strength of the composite causing the significant reduce in delaminated areas as shown in Figs. 13 and 14 as compared to Fig. 10.

4 Conclusions

At this stage of findings for the ongoing research it was found that:

1. Introduced nanosized Al_2O_3 and TiO_2 particles produced together with stirring effect have shown a refining effect on the microstructure features of the A390 hypereutectic aluminium alloys where an obvious refining in the Si particles average size from 30–40 μm to 10–20 μm occurred.
2. The introduction of the nanosized particles led to an increase in hardness and micro-hardness of the A390 alloy from about 100 to 148 HB.
3. Significant changes have been found in the wear behaviour of the tested material after adding nanosized particles.
4. A combined intermetallic TiAlMgSi oxide was found in some regions after adding 1 % Al_2O_3 and 0.5 % TiO_2 nanoparticles.

Acknowledgments The present study was part of a big research project on developing nanodispersed cast light aluminium and magnesium alloys, for investigating options for enhancing their properties and performance in automotive applications. The project was supported by the facilities of: British University in Egypt BUE; Scientific and Technology Centre of Excellence Salam City; Department of Mechanical engineering Cairo University; Department of Mechanical Engineering Helwan University, Egypt; and the Gemeinshaftslabor fuer Elektronmikroskopie Aachen University, Germany. The exchange of visits between Egypt and Germany was funded by both Science and Technology Development Funding Office STDF and Deutsche Akademishe Austaush Dienst DAAD.

References

1. Haizhi, Y.: An overview of the development of Al-Si-alloy based material for engine applications. J. Mater. Eng. Perform. JMEPEG **12**, 288–297 (2003)
2. Gruzleski, J.E.; Closset, B.M.: The Treatment of Liquid Aluminium–Silicon Alloys. AFS, Des Plaines, pp. 107–126 (1990)
3. Shi, W.; Gao, B.; Tu, G.; Li, S.; Hao, Y.; Yu, F.: Effect of neodymium on primary silicon and mechanical properties of hypereutectic Al-15 %Si alloy. J. Rare Earths **28**, 367–370 (2010) (Spec. Issue)
4. Chen, C.; Liu, Z.; En, B.; Wang, M.X.; Weng, Y.; Liu, Z.: Influences of complex modification of P and RE on microstructure and mechanical properties of hypereutectic Al-20Si alloy. Trans. Nonferrous Met. Soc. China **17**, 301–306 (2007)
5. El-Mahallawi, I.S.; Shash, Y.; Eigenfeld, K.; Mahmoud, T.S.; Ragaie, R.M.; Shash, A.Y.; ElSaeed, M.A.: Influence of nanodespersions on strength—ductility properties of semisolid cast Al alloy. Mater. Sci. Technol. **26**(10), 1226–1231 (2010)
6. El-Mahallawi, I.; Abdelkader, H.; Yousef, L.; Amer, A.; Mayer, J.; Schwedt, A.: Influence of Al_2O_3 nanodispersions on microstructure features and mechanical properties of cast and T6 heat-treated Al Si hypoeutectic alloys. Mater. Sci. Eng. A **556**, 76–87 (2012)
7. Mazahery, A.; Baharvandi, H.R.; Abdizadeh, H.: Development of high performance A356-nano Al_2O_3 composites. Mater. Sci. Eng. A **518**, 23–27 (2009)
8. Zhao, J.; Wu, S.: Microstructure and mechanical properties of rheodiecasted A390 alloy. Trans. Nonferrous Met. Soc. China **20**, 754–757 (2010)
9. Tebib, M.; Morin, J.B.; Ajersch, F.; Grant Chen, X.: Semi-solid processing of hypereutectic A390 alloys using novel rheoforming process. Trans. Nonferrous Metals Soc. China **20**, 1743–1748 (2010)
10. Dehong, L.; Yehua, J.; Guisheng, G.; Rongfeng, Z.; Zhenhua, L.; Rong, Z.: Refinement of primary Si in hypereutectic Al–Si alloy by electromagnetic stirring. J. Mater. Process. Technol. **189**, 13–18 (2007)
11. Rohatgi, P.K.; Asthana, R.; Das, S.: Solidification, structure and properties of cast metal-ceramic particle composites. Int. Metals Rev. **31**(3), 115–139 (1986)
12. Rosso, M.: Ceramic and metal matrix composites: routes and properties. J. Mater. Process. Technol. **175**, 364–375 (2006)
13. Saha, D.; Apelian, D.: Semi solid processing of hypereutectic alloys. AFS Trans. **112**, 4–57 (2004)
14. Wannasin, J.; Thanabumrungkul, S.: Development of a semi-solid metal processing technique for aluminium casting applications. Songklanakarin J. Sci. Technol. **30**(2), 215–220 (2008)
15. Yousef, L.S.; Mahmoud, T.S.; Rashad, R.M.; Elmahallawi, I.M.: Effect of Mechanical stirring in mushy zone on the microstructural characteristics of A356 Al alloy. J. Eng. Appl. Sci. **53**(4), 557–572 (2006)
16. Kim, G.; Hong, S.; Lee, M.; Kim, S.; Ioka, I.; Kim, B.; Kim, I.: Effect of oxide dispersion on dendritic grain growth characteristics of cast aluminum alloy. Mater. Trans. **51**(10), 1951–1957 (2010)
17. Huda, D.; El Baradie, M.A.; Hashmi, M.J.S.: Metal matrix composites: materials aspects. Part II. J. Mater. Process. Technol. **37**, 528–541 (1993)
18. Khalifa, W.; Samuel, F.H.; Gruzleski, J.E.: Nucleation of solid aluminium on inclusion particles injected into Al–Si–Fe alloys. Metal. Mater. Trans. A **35A**, 3233–3250 (2004)
19. Tong, G.; Pengting, L.; Yunguo, L.; Xiangfa, L.: Influence of Si and Ti contents on the microstructure, microhardness and performance of TiAlSi intermetallics in Al–Si–Ti alloys. J. Alloys Compd. **509**, 8013–8017 (2011)
20. Alireza, H.A.; Frank, A.: Effect of conventional and rheocasting processes on microstructural characteristics of hypereutectic Al–

Si–Cu–Mg alloy with variable Mg content. J. Mater. Process. Technol. **210**, 767–775 (2010)
21. Alireza, H.A.; Xichun, L.; Frank, A.; Grant Chen, X.: Wear behaviour of hypereutectic Al–Si–Cu–Mg casting alloys with variable Mg contents. Wear **269**, 684–692 (2010)
22. ChandrasheKhairaiah, T.M.; Kori, S.A.: Effect of grain refinement and modification on the dry sliding wear behaviour of eutectic Al–Si alloys. Tribol. Int. **42**, 59–65 (2009)
23. Starink, M.J.; Abeels, V.M.F.; Van Mourik, P.: Lattice parameter and hardness variations resulting from precipitation and misfit accommodation in a particle-reinforced Al–Ai–Cu–Mg alloy. Mater. Sci. Eng. A **163**, 115–125 (1993)
24. Alpas, A.T.; Zhang, J.: Effect of microstructure (particulate size and volume fraction) and counterface material on sliding wear resistance of particulate-reinforced aluminum matrix composites. Metal. Mater. Trans. A **25A**, 969–982 (1994)
25. Zhang, Z.F.; Zhang, L.C.; Mai, Y.W.: Wear of ceramic particle-reinforced metal-matrix composites. Part I: wear mechanism. J Mater. Sci. **30**, 1961–1966 (1995)
26. Zhang, Z.F.; Zhang, L.C.; Mai, Y.W.: Wear of ceramic particle-reinforced metal-matrix composites. Part II: a model of adhesive wear. J. Mater. Sci. **30**, 1967–1971 (1995)
27. Amro Al-Qutub, M.: Effect of heat treatment on friction and wear vehavior of Al-6061 composite reinforced with 10 % submicron Al_2O_3 particles. Arab. J. Sci. Eng. **34**(1B), 205–215 (2009)